Colloids and Surfaces B: Biointerfaces 148 (2016) 640–649

Contents lists available at ScienceDirect

Colloids and Surfaces B: Biointerfaces

journal homepage: www.elsevier.com/locate/colsurfb

Langmuir films of dipalmitoyl phosphatidylethanolamine grafted poly(ethylene glycol). In-situ evidence of surface aggregation at the air-water interface

Eduardo M. Clop, Natalia A. Corvalán, María A. Perillo*

Instituto de Investigaciones Biológicas y Tecnológicas IIBYT (CONICET-UNC) Cátedra de Química Biológica, Depto de Química, FCEFyN, Universidad Nacional de Córdoba. Av. Vélez Sarsfield 1611, X 5016GCA Córdoba, Argentina

ARTICLE INFO

Article history:
Received 5 April 2016
Received in revised form 25 August 2016
Accepted 20 September 2016
Available online 20 September 2016

Keywords:
Polymer grafted lipids
PE-PEG
Mixing behavior
Langmuir films
PM-IRRAS
BAM
EFM
Surface aggregation

ABSTRACT

The molecular packing-dependent interfacial organization of polyethylene glycol grafted dipalmitoylphosphatidylethanolamine (PE-PEGs) Langmuir films was studied. The PEG chains covered a wide molecular mass range (350, 1000 and 5000 Da).

In surface pressure-area (π-A), isotherms PE-PEG^{1000} and PE-PEG^{5000} showed transitions (midpoints at $\pi_{m,t1} \sim 11$ mN/m, "**t1**"), which appeared as a long non-horizontal line region. Thus, **t1** cannot be considered a first-order phase transition but may reflect a transition within the polymer, comprising its desorption from the air-water interface and compaction upon compression. This is supported by the increase in the ν_s(C-O-C) PM-IRRAS signal intensity and the increasing surface potentials at maximal compression, which reflect thicker polymeric layers. Furthermore, changes in hydrocarbon chain (HC) packing and tilt with respect to the surface led to reorientation in the PO_2^- group upon compression, indicated by the inversion of the $\nu_{asym}(PO_2^-)$ PM-IRRAS signal around **t1**. The absence of a **t1** in PE-PEG^{350} supports the requisite of a critical polymer chain length for this transition to occur. In-situ epifluorescence microscopy revealed 2D-domain-like structures in PE-PEG^{1000} and PE-PEG^{5000} around **t1**, possibly associated with gelation/dehydration of the polymeric layer and appearing at decreasing π as the polymeric tail became longer.

Another transition, **t2**, appearing in PE-PEG^{350} and PE-PEG^{1000} at $\pi_{m,t2} = 29.4$ and 34.8 mN/m, respectively, was associated with HC condensation and was impaired in PE-PEG^{5000} due to steric hindrance imposed by the large size of its polymer moiety.

Two critical lengths of polymer chains were found, one of which allowed the onset of polymeric-tail gelation and the other limited HC compaction.

1. Introduction

Poly(ethylene glycol) (PEG), with different degrees of polymerization covalently bound to a phospholipid moiety, comprises a kind of lipopolymer (LP) widely used in liposome formulations for drug encapsulation and transport [5]. In these liposomes, PEG moieties are the polar head group and form a hydrophilic coating that stabilizes vesicles and increases their half-life in the circulatory system, preventing their self-aggregation and/or fusion as well as the nonspecific adsorption of serum proteins [6].

PEGylated phospholipids may also be important for building up model membranes containing a pseudo-glycocalix. Other lipids covalently modified with hydrophilic polymers, including glycolipids with both linear and branched head, were considered good candidates to build up a model glycocalix [7]; however, the complex interactions between these hydroxylated polymers and possible adsorbed molecules complicate the study of their properties in such complex chemical environments. The use of PEG derivatives would avoid this disadvantage, although it would require their being stabilized in a lamellar, near planar, phase.

It was proposed that linear polymers attached to interfaces may be found in two different organizational schemes depending on the packing density [8,9], i.e. a random coil (mushroom) conformation at a low molecular packing, and a stretched (brush) conformation at higher molecular packings. Moreover, on the basis of polymer physics [10], it was predicted that, according to the composition and the proportion of PEGylated phospholipids in mixtures with other phospholipids, it would be possible to achieve these two

* Corresponding author.
E-mail address: mperillo@unc.edu.ar (M.A. Perillo).

http://dx.doi.org/10.1016/j.colsurfb.2016.09.023
0927-7765/

conformations ("brush" or "mushroom") not only in monolayers but also in liposomes [11]. A third conformation, the pancake, has also been predicted to exist in monolayers at the lowest surface pressures [12,13]. In addition, theoretical models make it possible to predict the thickness of the polymer layer arranged near the lipid-water interface, as well as the conformational and rheological changes undergone by the polymer, which depend on the molecular packing of the monolayer where it is anchored both with phospholipid [14] and with O-linked alkyl glycerol derivatives [13].

There is considerable information in the literature about different PEG lipopolymer derivatives, studied with different perspectives, methods [8,14–20] and physical conditions [2,3,8]. However, a complete analysis of the same set of molecules in similar conditions through a combination of techniques is lacking. This would help to better understand the molecular features underlying the control of surface organization of these biopolymers.

Therefore, in the present paper, we used dipalmitoyl phosphatidylethanolamine (PE), covalently modified with three PEGs differing only in the number of monomer subunits (7, 23 or 113 subunits for PEG^{350}, PEG^{1000} and PEG^{5000}, respectively). The interfacial stability and the conformational equilibrium of LP were studied by lateral pressure vs. area (π-A) compression isotherms. Brewster angle microscopy (BAM), epifluorescence microscopy (EFM) and polarization modulation infrared reflection-absorption spectroscopy (PM-IRRAS) were combined, in conjunction with Langmuir balance experiments with different molecular packing conditions and at constant temperature, to evaluate the transitions occurring within both the lipid hydrocarbon chains (HC) and the polymer.

Note that, although Langmuir trough experiments have been widely applied to study the behavior of similar LPs at the air-water interface, the LP series studied in the present work have not been included in previous reports. This information not only completes already existing information, but is also useful to understand microscopic and spectroscopic data, which are the novel contributions of the present work.

2. Materials and methods

2.1. Materials

1,2-dipalmitoyl-sn-glycero-3-phosphoethanolamine-N-[methoxy(polyethylene glycol) with average PEG molecular weights of 350, 1000 and 5000 (PE-PEG^{350}, PE-PEG^{1000}, PE-PEG^{5000}) were purchased from Avanti Polar Lipids (Alabaster, Alabama). DiI-C_{18}, 1,1′-dioctadecyl-3,3,3′,3′-tetramethylindocarbocyanine perchlorate was from Molecular Probes Inc. (Eugene, OR, USA). The general structure of the three PE-PEGs analyzed is summarized in Fig. S1 (Supplementary data).

2.2. Surface pressure vs mean molecular area (π-A) compression isotherms

2.2.1. π-A isotherm recording

Monomolecular layers were prepared and monitored with a Minitrough II (KSV Instruments Ltd., Finland) (see Supplementary data and ref [21]. for a detailed description). Briefly, $CHCl_3$:MeOH (2:1) solutions of pure compounds were spread on an unbuffered aqueous surface at $25 \pm 1\,^{\circ}C$. The interface was compressed at a 10 mm^2/s constant compression rate. Lateral surface pressure (π) was measured by the Wilhelmy plate method and the surface potential (ΔV) registered simultaneously by the voltage-measuring system (vibrating plate method; KSV Instruments, Helsinki, Finland). Reproducibility was within ± 0.01 nm^2, ± 1 mN/m and ± 1 mV for molecular area (A), π and ΔV, respectively.

The surface parameters A_{min} (minimum A occupied by an amphipathic molecule in a monolayer at the closest molecular packing) and π_c (collapse pressure, the maximal π corresponding to A_{min}), were obtained from π-A isotherms.

2.2.2. Compression modulus

The compression modulus K was calculated for each isotherm according to Eq. (1):

$K = -(A_\pi) \cdot \left(\frac{\delta\pi}{\delta A}\right)_T$ [1]

where A_π is the molecular area at π. K enables the elasticity of the monolayer to be inferred, and the bidimensional phase transitions from the π-A isotherm profile to be defined more precisely.

2.2.3. Molecular area for the onset of a hypothetical mushroom–brush phase transition

For a surface-grafted polymer in a "mushroom" regime, the global approximation theory of Flory-Huggins was used [10] (for calculation details see Supplementary data).

2.3. Brewster angle microscopy (BAM) and epifluorescence microscopy (EFM)

A Brewster angle microscope (EP^4, Nanofilm, Germany) was mounted over a Langmuir trough for direct interfacial observation. During isotherm compression, π was stopped at the desired value (5, 15 or 35 mN/m) and 5 min were allowed for film stabilization. BAM images were obtained through a 10× objective with 2 μm lateral resolution and were recorded with a CCD camera.

For EFM experiments, monolayers were prepared from solutions doped with 1 mol% DiI-C_{18}. A KSV Minisystems surface barostat was mounted on the stage of a Nikon Eclipse TE2000-U (Tokyo, Japan) microscope, which was supplied with 20 × long-working distance optics. The Teflon trough used had a 35-mm diameter quartz window at its base, which allowed the monolayer to be observed through the trough. The monolayer morphology was documented with a Nikon DS–5 M color video camera supporting a resolution up to 2560–1920 pixels, which represents 1231 × 923 μm (Capture area).

2.4. PM-IRRAS spectroscopy

Polarization Modulation Infrared Reflection-Absorption Spectroscopy (PM-IRRAS) was performed essentially as described previously [21] (see also Supplementary data), with a KSV PMI 550 PM-IRRAS (KSV Instruments Ltd., Finland) mounted on a KSV Minitrough.

Spectra were collected with a resolution of 8 cm^{-1}, at 100 kHz modulating frequency and a variable delay in the wavelength (λ). The incidence angle was 80° and the maximum retardation wavelength was 1500 cm^{-1} with a gap of 0.55λ. These parameters enabled a high resolution IR spectrum to be recorded within the 950 and 1900 cm^{-1} wavenumber range in which most signals from phospholipids and PEG polar heads appeared. For an incidence angle of 80°, a positive-oriented band indicates a transition moment occurring preferentially in the plane of the surface, while a negative downward-oriented band reveals an orientation preferentially perpendicular to the surface [22]. The integrated absorption (I) of a peak reflects both the orientation of the molecules and the total number of molecules in the IR beam [23]. Hence, the product *I.A* would be expected to be constant during the compression, provided there is no molecular reorientation during the compression. This was applied to the analysis of PO_2^- peak reorientation.

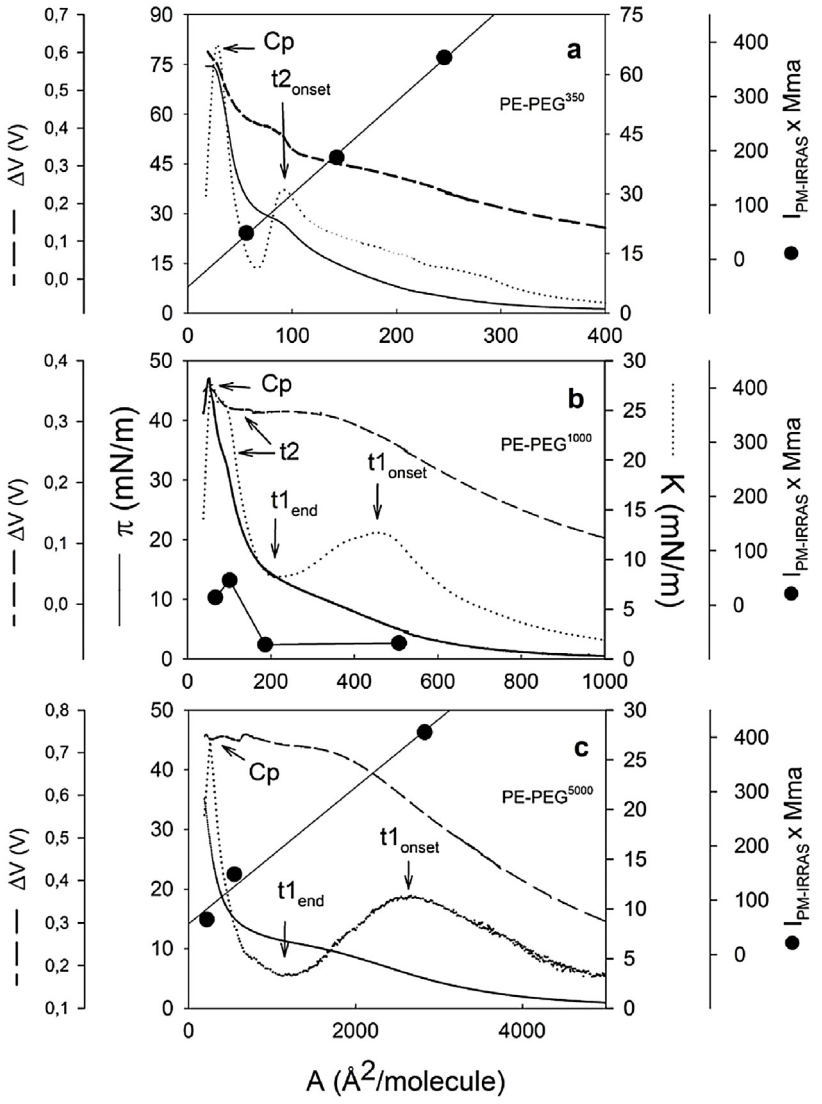

Fig. 1. Surface pressure (——, π), compression modulus (·····, K) and surface potential (-----, ΔV) vs. molecular area (A) isotherms of PE-PEG^{n} at the air-water interface. PE-PEG^{350} (a), PE-PEG^{1000} (b) and PE-PEG^{5000} (c) were compressed up to their collapse pressure (π_c); K was calculated from (ec.1); ●, IxA of $\nu_{as}(PO_2^-)$ signal in PM-IRRAS spectra (see Section 3.2). Arrows point to the collapse point (Cp) and to transitions (t1 and t2). $t1_{onset}$ and $t1_{end}$ refer to the start and the complexion of this transition. Data shown correspond to representative experiments replicated 2–5 times. Reproducibility was ±0.01 nm^2, ±1 mN/m and ±10 mV for A, π and ΔV, respectively. Temperature 25 ± 1 °C.

3. Results and discussion

3.1. Langmuir films: π-a compression isotherms

PE-PEGs were able to form stable and compressible films at the air-water interface (Fig. 1a–c, full lines). Monolayers exhibited highly expanded π-A isotherms and achieved a coherence (lift-off point) at molecular areas ($A_{lift\text{-}off}$) that increased with the PEG molecular mass ($A_{lift\text{-}off}$: 660, 1000 and 6000 Å^2/molecule for PE-PEG^{350}, PE-PEG^{1000} and PE-PEG^{5000}, respectively). With the increase of molecular mass, a decreasing π_c (60, 55, 28 mN/m) and an increasing A_{min} (39, 58, 250 Å^2/molecule) were observed for PE-PEG^{350}, PE-PEG^{1000} and PE-PEG^{5000}, respectively.

The π_c behavior reflected an increase in film instability associated with the high hydrophilic/hydrophobic ratio in the molecular structure of LP. Moreover, at its closest packing, PE-PEG^{350} achieves a molecular density similar to regular phospholipids, indicating that the polar region was able to elongate almost completely along the normal to the membrane. The other PE-PEGs had larger polar groups. Particularly in PE-PEG^{5000}, the A_{min} is significantly larger than the A_{min} of two tightly packed HC [24], indicating that the polymer moiety is not fully extended along the normal to the monolayer surface, adopting a molecular cone-shape geometry due to the huge size of the polar head. This imposes a steric hindrance to packing and destabilizes the monolayer, as evidenced by its lower π_c.

3.2. Langmuir films: K-A compression isotherms

Fig. 1a–c also depict K-A plots (dotted lines) corresponding to the π-A isotherms. High K value (low compressibility) means that molecules are tightly packed and the cohesive forces are considerable. K can also be employed to categorize the state of Langmuir monolayers. In gaseous monolayers, the *K* value is of the same magnitude as the π, while for liquid-expanded (LE) films it ranges from 12.5 to 50 mN/m and the liquid-condensed (LC) state is characterized by higher K values (within the limits of 100–250 mN/m), according to Davies and Rideal's criterion [25]. Assuming this criterion is still applicable to LP, only PE-PEG^{350} reached a π compatible

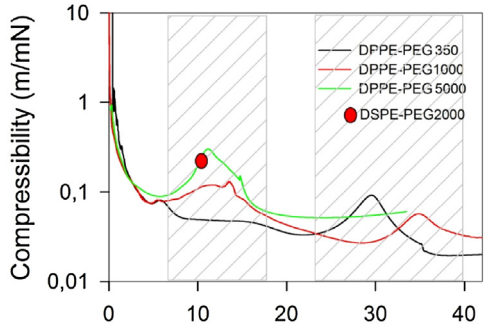

Fig. 2. Compressibility as a function of surface pressure. DPPE-PEG^{350} (black), DPPE-PEG^{1000} (red) and DPPE-PEG^{5000} (green) around the low- and high- pressure transitions (shaded regions). Red circle, data from ref. [2]. (For interpretation of the references to colour in this figure legend, the reader is referred to the web version of this article.)

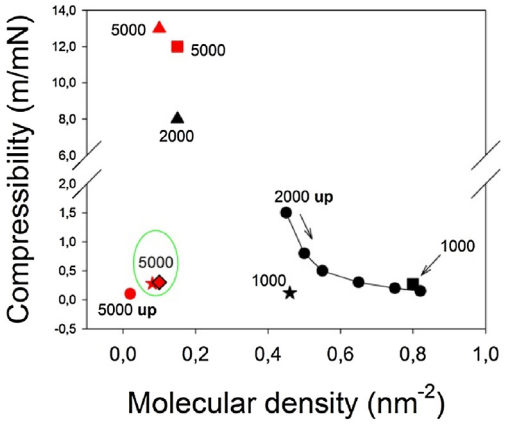

Fig. 3. Variation of (K^{-1}) as a function of molecular density (A^{-1}). Data at the low (black symbols) and high (**red** symbols) π transitions correspond to D**P**PE-PEG^n derivatives taken from the present work (★, ★) or to D**S**PE-PEG^n derivatives taken from the literature: [8] (●, ● , ▲, ▲); [3] (■, ■) and [2] (◆). Numbers refer to the molecular mass (n) of the PEG moiety. **2000 up**, data obtained at the high π transition of DSPE-PEG^{2000} at different temperatures (T). Arrow points in the direction of increasing T within the 281–307 K range. The other experiments were performed at 288–293 K. There are similarities between the present work and ref [2]. data (green circle). (For interpretation of the references to colour in this figure legend, the reader is referred to the web version of this article.)

with a LC state. Significant changes in film elasticity were detected through K-A isotherms (Fig. 1). The onsets of two types of transition, identified as "**t1"** and "**t2"**, were detected at maxima in K-A isotherms. "t1" appeared at low π in PE-PEG^{1000} and PE-PEG^{5000} (6.5 and 5.7 mN/m, respectively) and "t2" appeared at high π in PE-PEG^{350} and PE-PEG^{1000} (26 and 33 mN/m, respectively).

Instead of K-A plots, which are usually applied to analyze lipid monolayers, compressibility data ($C = K^{-1}$) are more frequently reported within the lipopolymer area. In particular, a C vs. π plot is a kind of phase diagram allowing a qualitative identification of the different types of transition and the simultaneous comparison of the behavior of several LP molecules with highly dissimilar molecular areas (Fig. 2). Transition midpoints (π_m) can be determined from maxima in compressibility vs.π plots (see below), and were $\pi_{m,\mathbf{t1}} \sim 11$ mN/m for PE-PEG^n with $n = 1000$ and 5000 and $\pi_{m,\mathbf{t2}} = 29.4$ and 34.8 mN/m, for PE-PEG^{350} and PE-PEG^{1000}, respectively. It is interesting to note in Fig. 2 that, at the completion of t1 ($\pi \sim 18$ mNm), PE-PEG^{1000} and PE-PEG^{5000} exhibited similar compressibility values (~0.051 and 0.058 m/mN), suggesting that they were in a similar phase organization.

Compressibility data found in the literature are related mainly to the D**S**PE-PEG series and exceptionally to D**P**PE-PEGs, and are quite diverse in terms of assay temperatures and values. Many works are aimed at understanding the contribution of the lipid moiety to the network formation of LP, so they center their attention only on the strength of alkyl chain condensation (high π transition) for the different MW systems studied (Fig. 3). The only comparison we can make with published data is that C values determined for DPPE-PEG^{5000} in the present work are of the same order of magnitude as that for DSPE-PEG^{5000} reported previously [2].

3.3. 2D-transitions

"t1" appeared as a non-horizontal line region (a pseudo-plateau), which is inconsistent with a first-order phase transition or with the coexistence of two thermodynamic phases. Using the grafted polymer theory, "t1" has been attributed to a conformational polymer transition from "pancake" to "mushroom" conformations [11,15]. It has also been associated with polymer desorption from the air-water interface and was found only if polymer chains showed an amphiphilic character [14]. Here we show that, in addition to hydrophilicity, a sufficient length of the hydrophilic tail is also required for t1 to be observed.

A hypothesis not considered in the literature in association with "t1" is the possibility that the stretching of the polymer chain may be accompanied by its desorption as a continuous process, which can be rationalized as a pancake-mushroom-pseudo brush transition. According to the Flory-Huggins theory for surface-grafted polymers at the low density limit of grafting points, each chain occupies roughly a half-sphere, with a truncated diameter comparable to the Flory radius (R_F) for a coil in good solvent. When, upon compression, the distance between the grafting points (D) approximates to R_F, polymers start an elongation perpendicular to the attaching interface and toward the bulk phase, thus entering a brush (or pseudo-brush) regime. However, as proposed earlier, the pancake state appears prior to the "mushroom" conformation. From the length and number of monomers in each lipopolymer, R_F can be calculated (Eq. (3) Supplementary data, [12,13]) and used to predict the molecular area at which the theoretical mushroom-to-brush transition is expected to start. Interestingly, the results obtained for PE-PEG^{1000} (417 Å^2/molecule) and PE-PEG^{5000} (2800 Å^2/molecule) are close to "t1". In the case of PE-PEG^{350}, the theory predicts a transition at 99 Å^2/molecule. Although this transition is not evidenced in the PE-PEG^{350} π-A isotherm, this theoretical value is also close to the "t2" for this lipopolymer (see below).

In turn, two hypothetical self-organization models from the literature may explain "t2". As *a first hypothesis*, "t2" may correspond to conformational changes experienced within the polymers, e.g., from pseudo-brush to brush, or mushroom to brush [8]. As *a second hypothesis*, "t2" may be a "native" transition of the lipopolymer that can be seen only when the lipid and polymer coexist in the same molecule. Thus, although requiring the presence of the polymer tail, "t2" took place within the lipid HC [8,9,14,18]. This second hypothesis is a conclusion from π-A compression isotherms at different temperatures and from IRRAS of LP with saturated and unsaturated HC [14]. This was supported through IRRAS of LP with deuterated lipid alkyl chains, analyzing the signals of symmetric (ν_s) and asymmetric (ν_{as}) stretching of hydrogenated (CH_2) and deuterated (CD_2) methylene groups [18]. Also, Langmuir film studies with copolymers built up by two blocks, one hydrophobic (polystyrene, PS) and one hydrophilic (polyethylene oxide, PEO), revealed a "t1" but not a "t2" transition [9].

Thus, our results contribute to support the second hypothesis for "t2", as we observed that this transition occurred only with PE-PEG^{350} and PE-PEG^{1000} but not with PE-PEG^{5000}. Cohesive interactions within HC can thus be impaired by steric hindrance imposed by large polymer moieties. However, while "t2" was absent in the PE-PEG^{5000} used in the present work (dipalmitoyl-PE-PEG^{5000}),

distearoyl-PE-PEG^{5000}, having HCs two carbons longer, exhibited a "t2" at 18 mN/m [26]. Our results highlight that, at some point, the hydrophilic/hydrophobic balance required for the occurrence of t2 is subtle.

3.4. Langmuir films: ΔV-A compression isotherm analysis

From this experiment, both the magnitude of ΔV and the shape of the isotherms provide important information. ΔV (Fig. 1a–c, dash line) was always positive, increased with compression, and exhibited clear slope changes at "t2" in PE-PEG^{350} and PE-PEG^{1000}, reaching a plateau at the end of "t1" in PE-PEG^{1000} and PE-PEG^{5000}. This indicates that molecular packing was accompanied by reorientation of functional groups. This is supported by data from PM-IRRAS experiments showing changes in the magnitude of IxA for PO_2^- vs. A (Fig. 1a–c, black dots) (see details in Section 3.5).

The magnitude of ΔV, at the plateau of the ΔV–A isotherms, increased from 0.300 ± 0.014 V (N = 3) in PE-PEG^{1000} to 0.700 ± 0.016 V (N = 6) in PE-PEG^{5000}. Interestingly, the change in ΔV (ΔΔV) along the t1 transition (Fig. 1) in PE-PEG^{5000} (∼110 mV) was almost double that in PE-PEG^{1000} (∼40 mV). ΔV values are dependent on the component normal to the monolayer of the net dipole moment ($\mu_\perp$) of the molecules at the interface and can be decomposed into contributions from hydrocarbon chains (HC) of esterified fatty acids, phospholipid head groups, polymer moiety and structured water molecules. In turn, ΔΔV roughly reflects dipole reorientation accompanying a π change. The HCs $\mu_\perp$ is positive [24] and, upon compression, is expected to contribute a higher ΔΔV in PE-PEG^{1000} than in PE-PEG^{5000}, because the former would be more vertically oriented than the latter at the same π, due to the lower steric hindrance of its polymeric group (Fig. 5c). In spite of this, the highest net ΔΔV was obtained with PE-PEG^{5000}, which may be attributed to its thicker polymeric layer.

3.5. Surface topography of PE-PEG langmuir films

Surface topography of PE-PEG Langmuir films at different π were imaged in-situ by BAM and EFM (Fig. 4). EFM and BAM images display different information. BAM reflects contrasts in refractive indices. Brighter areas correspond to thicker phases, which correlate with an elongation due to a conformational (rheological) transition within the region of the polymer moiety of LP. In turn, EFM-imaged topography reflects the differential partitioning and/or spectroscopic behavior of the fluorescent probe in the different coexisting phases.

3.5.1. BAM-imaged topography

At all the π studied, PE-PEG^{350} films (Fig. 4a–c) showed homogeneous BAM images, and PE-PEG^{1000} films a grainy texture with bright circular domains of ≅9 μm diameter (Fig. 4d–g). Something similar was observed in PE-PEG^{5000} monolayers, but here the circular dots appeared at 15 mN/m and remained up to the highest pressures studied (Fig. 4h–j). In all samples, the background of BAM images was homogeneous and became brighter upon compression, indicating the thickening of the monolayer mainly due to desorption from the interface into the subphase and stretching of the LP polymeric tails. Furthermore, grains, when present, did not grow, coalesce or appreciably increase their surface density at the highest pressures.

The existence of non-satisfied hydration and/or spreading lag times before the starting of the compression was excluded as an aggregation source (Fig. S4, Supplementary data). Such structures may also be considered as metastable aggregations of small domains or of other types of finite-sized domains, e.g. domains whose molecules or head groups are simply oriented differently from those in the surrounding phase, or surface aggregating structures that are in equilibrium with a preexisting monolayer or submonolayer. Structures of similar shapes were interpreted as budding collapsed structures when observed in DSPE-PEG^{5000} monolayers [26], as liquid crystalline domains in DPPE monolayers spread from chloroform solutions [27] or just as dense domains in polystyrene-polyethyleneoxide (PS-PEO) copolymers [9]. Here, we propose that bright domains are nucleation points, while the interdomain space is occupied not only by polymer chains from molecules located at domain borders but also by other PE-PEG^n molecules not included in the condensation nuclei. This prevents domains growing or approaching each other upon compression.

3.5.2. EFM-imaged topography

EFM of PE-PEG^{350} exhibited some roughness at 5 and 15 mN/m (Fig. 4a′–4b′), which were seen as dark domains at 35 mN/m (Fig. 4c′). In PE-PEG^{1000}, EFM exhibited domains that were dark at 15 mN/m (Fig. 4e′), bright at 25 mN/m (Fig. 4f′) and percolated at higher π (Fig. 4g′). Finally, in PE-PEG^{5000}, EFM showed bright domains at 5 mN/m (Fig. 4h′), which were percolated at higher π (Fig. 4i′ and j′).

The fluorescent probes used in EFM have chemical structures resembling that of the lipid moiety of the LP (see Fig. S2, Supplementary data). In lipid membranes, the saturated long-chain DiI derivatives, such as DiIC18, follow a preferential partitioning and show a higher molecular brightness in liquid-ordered (Lo) than in liquid-disordered (Ld) phases [28]. However, since the fluorescent moiety of DiIC18 is located at its polar head group, in LP monolayers, the DiIC18 probe is expected to sense the physicochemical properties of the subphase, i.e. a PEG layer, in addition to the HC organization. The polymeric region of LPs at increasing compactness can be simulated with PEG MW 6000 (PEG^{6000}) solutions of increasing concentrations. In these solutions, DiIC18 exhibits a blue shift in its center of spectral mass and an increase in fluorescence intensity (see Fig. S3, in Supplementary data). This behavior resembles the effect of an environment with decreasing polarity, which is expected to occur with increasing [PEG^{6000}] [29] or PE-PEG^n surface density [30], due to the dehydration associated with compaction. So, in EFM images of LP monolayers, dark regions would represent highly disordered and/or hydrophilic zones, where the probe is excluded and/or exhibits low quantum efficiency, while brighter regions are associated with more compact polymeric chains producing a more hydrophobic environment.

We can therefore propose that, in PE-PEG^{1000} and PE-PEG^{5000} monolayers, regions at which PEG tails are sufficiently concentrated and packed below the HC sheet provide a dehydrated environment, evidenced as brilliant red domains, which coexist with other less brilliant (more hydrophilic) regions containing less-packed polymeric tails. These topographic patterns are indirectly associated with transitions, because they appear at π ≥5 mN/m in PE-PEG^{5000} and at π ≥25 mN/m in PE-PEG^{1000}, i.e., at and above the onset of their respective "t1", and they coalesce at higher π.

3.5.3. Ex-situ and in-situ LP monolayer imaging

It is noteworthy that most of the topographic data of LP of diblock co-polymer monolayers arises from ex-situ experiments (e.g., monolayers transferred onto solid substrates), using techniques such as AFM and grazing incidence X-ray diffraction (GID), which inspect the topography at a scale lower than in the present work [31]. Aggregation associated to "t2" has previously been proposed for DSPE, substituted with PEGs of 44 and 112 monomer-length through GID data and defined as 2D-micelles, consisting of tightly packed HC intercalated between PEG chains [32]. However, these structures consisted of 2D-nanostripes with a 12 nm periodicity, resulting from monolayers transferred onto mica and imaged ex-situ by AFM [32].

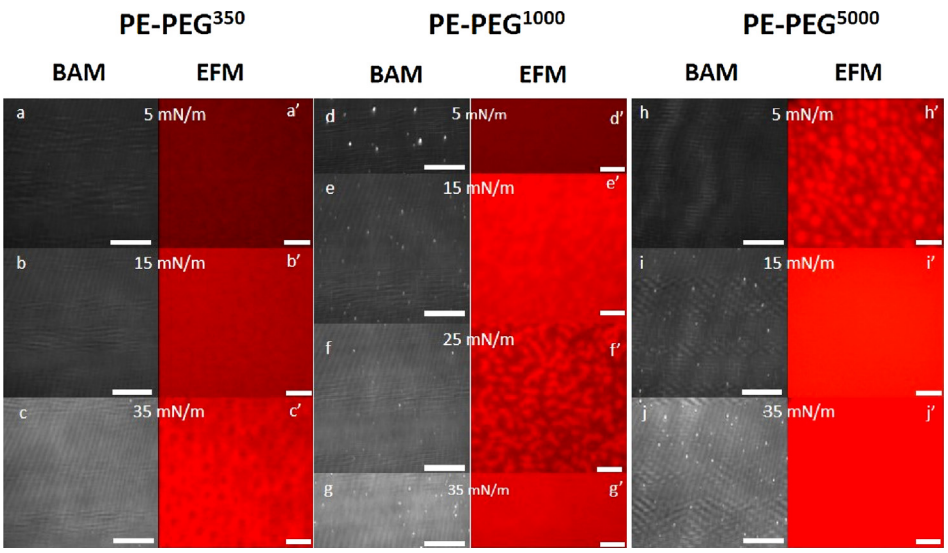

Fig. 4. Topographic analysis of lipopolymer monolayers. BAM and EFM images obtained from Langmuir films of PE-PEG^{350} (a–c,a′–c′), PE-PEG^{1000} (d–g, d′–g′) or PE-PEG^{5000}(h–j, h′–j′). Images were captured at the p indicated in the figure. White bar represents 100 μm. Experimental details are described in Section 2.3.

Most in-situ evidence for the existence of copolymer aggregates at the air-water interface and comes from rheological experiments. It is accepted that the "t2" transition is triggered by alkyl chain condensation, linked to the formation of surface micelles at the air-water interface, and leads to 2D-gelation [33]. This phenomenon involves a physical network among PEG LPs, with a relative strength depending on the MW of the polymeric moiety. This suggests that a sufficient strength of cohesive interaction within the hydrophobic moiety is necessary to form stable 2D gel [3], and that this would be impaired if there is a sufficient cross-sectional area mismatch (cone-shape) between polymer and lipid moieties. In-situ BAM images (large bright grains), observed in DSPE-PEG^{5000} monolayers at π above a high-π transition, were associated with monolayer collapse [26], while further π increases were considered over-compressed states. The different behavior, both in BAM and in π-A isotherms, observed here with DPPE-PEG^{5000} having a 2-carbons shorter HC, suggests that a HC/polymer balance is driving these transitions.

3.6. Surface spectroscopy

PM-IRRAS spectra of PE-PEGs in Langmuir films were recorded at different molecular packings during the monolayer compression (Fig. 5). Our analysis focused on the 950–1900 cm^{-1} wavenumber range of the IR spectra since, in addition to the complex vibrations band of the C—O—C skeleton of PEG around 1100 cm^{-1} [34,35], it also includes spectral bands characteristic of phospholipids.

Reference PM-IRRAS spectra were recorded of pure dpPE in Langmuir films at several π (Fig. 5a) and compared with an IR-ATR spectrum of dry dpPE taken from the literature (Fig. 5b). Major bands in the IR-ATR spectrum corresponded to ($u_{as}(PO^{-}{}_2)$, $\delta(CH_2)$, $\nu b(NH_3{}^+)$ and $\nu_s C{=}O$), with frequencies located at 1220, 1467, 1540 and 1740 cm^{-1}, respectively [1].

The PM-IRRAS spectrum of dpPE at the air-water interface (Fig. 5a) differed from dpPE on hydrophobic silicon (two-layers) (ATR in Fig. 5b), in:

a) The derivative shape of the band, due to the C=O stretching vibration near 1740 cm^{-1} and to a dip at 1660 cm^{-1} at defined π values.

In phospholipid bilayers, the *sn*-1 and *sn*-2 ester C=O groups are similarly oriented with respect to the bilayer plane, with an angle ≥60° relative to the bilayer normal, independently of hydration or phase state [36]. However, in Langmuir films, rotation of the whole molecule upon compression may explain an increase in the intensity of the $\nu_{as}(C{=}O)$ signal at 1740 cm^{-1} (becoming more horizontally oriented) (Fig. 5a).

The combination of a maximum at 1740 cm^{-1} and a minimum at 1660 cm^{-1} is the most striking feature in the PM-IRRAS spectra of phospholipids, which does not appear in the ATR spectrum (Fig. 5b). It has been shown that such a shape of a PM-IRRAS band can be observed when the transition moment of the vibration associated with the band is oriented at the PM-IRRAS "magic angle" with respect to the normal of the water surface (approximately 40°) [22]., The dip located at 1660 cm^{-1} has alternatively been defined as an optical effect peculiar to IRRAS, due to the strong dispersion of the refractive index of water in this spectral range (this dispersion has been ascribed to the bending mode δH_2O) [22,37,38] or the scissoring mode (δOH_2) of liquid water [39,40]. Previous numeric simulations have showed that, at a first approximation, this dip is proportional to the layer thickness at the water surface [37] and the refractive index of the media at the interface. This is important for understanding PEGylated PE spectra.

b) Increase in the frequency of $\nu_{as}(PO_2{}^-)$ band (1253 cm^{-1})

dpPE unlike other phospholipids, has the ability to form intra- and intermolecular hydrogen bonds [41]. The amine groups in dpPE prefer to hydrogen-bond with lipid oxygens and, in this process, the P-N vector of the dpPE headgroup is most often found pointing toward the bilayer core, while in N-substituted phospholipids such as PC, the P-N vector points toward the water phase [42]. Shifts in the positions of some peaks were found, associated with changes in the hydrogen bond pattern that characterizes the intermolecular network of dpPE at the interface [43]. There is evidence that the signal for the asymmetric stretching of free oxygen in the phosphate group ($u_{as}(PO^{-}{}_2)$), as well as that for the symmetric stretching of the carbonyl group ($\nu_s C{=}O$), move toward higher wavenumbers when the dpPE headgroup is dehydrated (not hydrogen-bonding with water) [44], e.g. it increases ~30 cm^{-1} for $u_{as}(PO^{-}{}_2)$ when the lipid is dehydrated [45]. In contrast, the shift of this band toward

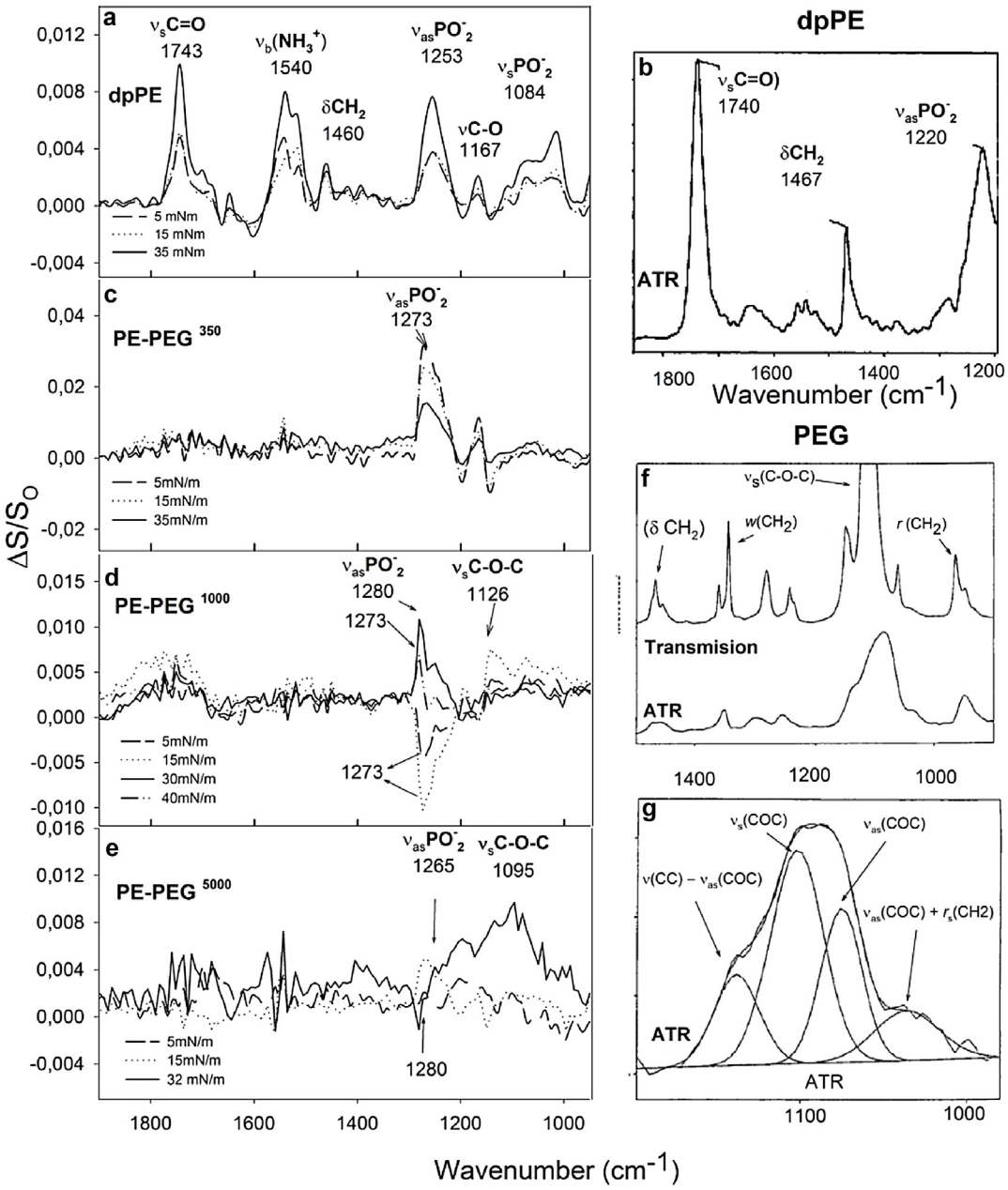

Fig. 5. FT-IR spectra. (a) PM-IRRAS of a dpPE monolayer; (b) ATR-FTIR spectrum of two layers of dpPE on hydrophobic silicon (Reprinted from ref. [1]. Copyright 1992 with permission of American Chemical Society) showing the three main vibrational modes of dpPE; (c), (d) and (e): PM-IRRAS of monolayers composed of PE-PEG350, PE-PEG1000 and PE-PEG5000, respectively, at different π (replicated at least twice with similar results; approximation error ±8 cm-1); f) ATR-FTIR spectrum of a PEG film immersed in a 1 mM NaCl solution (lower curve) and transmission FTIR spectrum of the same dried film (upper curve); g) Zoom-in on the lower spectra shown in f), magnifying the ‘fingerprint’ region of PEG (vibrational modes of C—O—C) (f and g were reprinted from ref. [4], Copyright 1996, with permission of Elsevier). ν, δ, r and w represent stretching, bending, rocking and wagging vibrational modes, respectively.

lower wavenumbers when it is hydrated is associated with the hydrogen-bonding of phosphate groups with water [45].

3.6.1. *General features of PM-IRRAS spectra from PEG derivatives*

PM-IRRAS spectra of the three LP studied are shown in Fig. 5c–e. Compared with dpPE at the air-water interface (Fig. 5a), the main difference observed with PE-PEGs is the absence of the band at 1540 cm^{-1} corresponding to a free $\nu b(NH_3^+)$ group. Moreover, at all π, these spectra were compatible with disordered or tilted HC (PM-IRRAS signal around 1460 cm^{-1} with an intensity too low or absent). The band at 1740 cm^{-1} due to ν_{as}(C=O), lost in PE-PEG^{350} and recovered in PE-PEG^{1000}, may be associated with a higher flexibility of the longer polymeric chain, allowing an increase in the horizontal component of the C=O transition moment.

PEG also exhibits a spectral region known as the “fingerprint”, corresponding to C—O—C vibrational modes of the polymer chain in an amorphous, non-crystalline structure [18], as shown in Fig. 5f and g (taken from [4]). The absorption maximum is influenced by the polarity of the environment, i.e. it is sensitive to the degree of phase hydration [35]. A swollen random coil structure (Fig. 5f, bottom curve, and Fig. 5g) differed from the narrow peaks characteristic of the dry bulk crystalline state (Fig. 5f, upper curve). Moreover, significant band shifts to lower frequencies are observed due to hydrogen bonding of water with the ether oxygen [4,46]. Similar to the behavior of PS-PEO copolymers, PE-PEGs did not

a

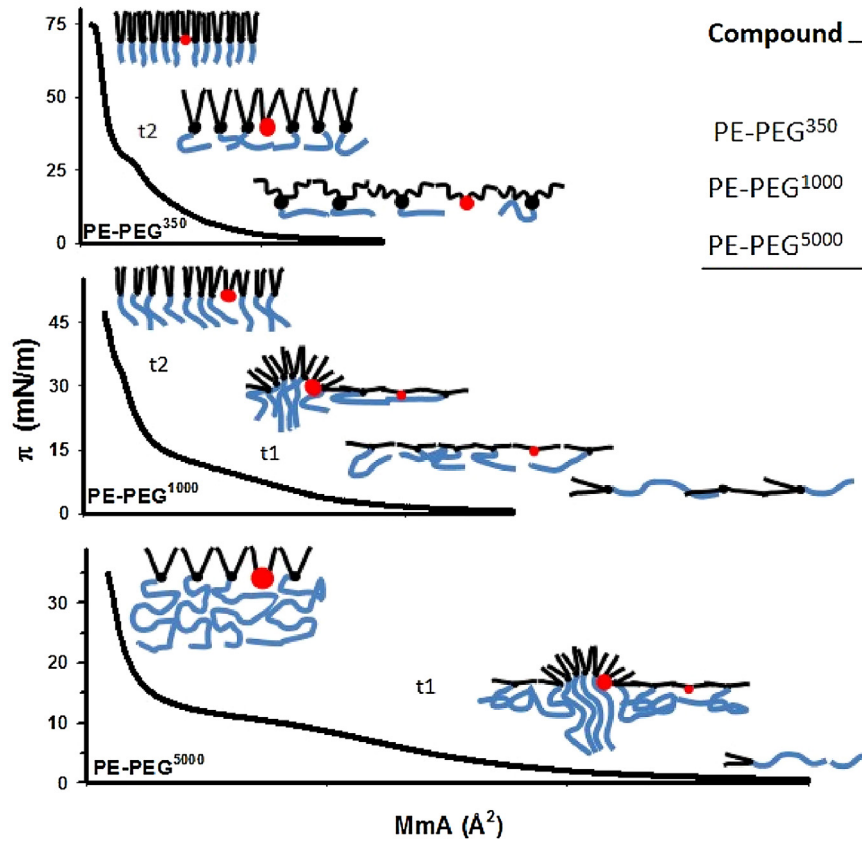

b

Compound	π (mN/m)			Molecular area (nm²/molec)		
	t1	t2	π_c	t1	t2	A_{min}
PE-PEG^{350}	-	25	60	-	0.97	0.37
PE-PEG^{1000}	6.5	32	55	4.5	0.96	0.58
PE-PEG^{5000}	10	-	42	15.8	-	1.88

c

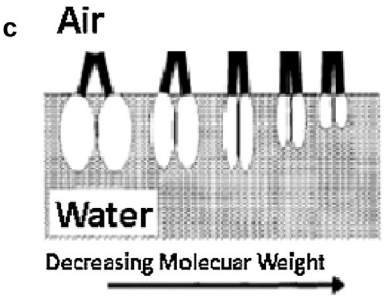

Fig. 6. a) Proposed models for lipopolymer organization along the π-A compression isotherms.
a) **Top**, PE-PEG^{350} homogeneous topography with hydrocarbon chain condensation at "t2". **Middle**, PE-PEG^{1000}, desorption of the polymer moiety from the interface at "t1" (pancake-mushroom transition) and formation of 2D-aggregates, evidenced when DiIC18 (red circles) is wrapped up within condensed and dehydrated PEG chains; condensation of hydrocarbon chains at "t2". **Bottom**, PE-PEG^{5000}, similar to PE-PEG^{1000} with a "t1" and 2D-aggregate topography reached at a lower π and absence of "t2" due to steric hindrance imposed by the higher MW polymer, preventing lipid chain condensation.
b) Summary of collapse and transition π values of PE-PEGs. Data shown correspond to the mean of 4–5 replicates and%CV were 4 ± 2% and 6 ± 5% for π and A, respectively.
c) Impairment in the intermolecular interactions within the hydrocarbon chains at high π increases as a function of the polymer moiety size. Adapted with permission from ref. [3]. Copyright 2002. ACS.

exhibit an inversion in the sign of the PM-IRRAS signal of the C—O—C group [9].

The fingerprint band of PEG superimposes with the ester CO—O single bonds (~1178 cm^{-1} [36]) and the $\nu_s PO_2^-$ (1080 cm^{-1} in dpPE). In bilayers, where the HC of phospholipids are on average oriented perpendicular to the bilayers, the CH2CO—OC fragment of the *sn*-1 chain is oriented in the direction of the all-trans methylene chain, while the same molecular segment of the *sn*-2 carbon chain is directed toward the bilayer plane. In monolayers, the orientation of functional groups is not constant because the entire molecule reorients upon compression. This should be taken into account when analyzing PM-IRRAS spectra.

3.6.1.1. PE-PEG^{350}. The PE-PEG^{350} spectrum (Fig. 5c) was quite conserved with respect to pure dpPE within the wavelength range 1150–1300 cm^{-1}, which includes one of the main vibrational modes corresponding to the $u_{as}(PO^-_2)$ around 1220 cm^{-1} (Fig. 5f). The absence of the vibrational mode of $\nu_b(NH_3^+)$ (1540 cm^{-1}) is expected because, in the LP, this group is involved in the amide bond with PEG. Neither the peaks corresponding to δCH_2 (1460 cm^{-1}) and ν_sC=O (1740 cm^{-1}) of the dpPE spectrum nor the characteristic peaks of PEG around 1100 cm^{-1} are observed in PE-PEG^{350} (Fig. 5c). It should be noted that, in PM-IRRAS, the absence of a peak in a spectrum does not necessarily indicate the lack of a functional group, but may be due to a difference in the orientation of a transition dipole with respect to the normal of the membrane [22], or to a random distribution (not oriented) of the absorption moments, which can also cause this effect [40]. In addition, the $u_{as}(PO_2^-)$ signal (Fig. 3c) exhibited a positive increase in peak amplitude upon compression, which suggests chain ordering and a rotation of PO_2^- transition moment towards a horizontal orientation.

3.6.1.2. PE-PEG^{1000}. In the case of PE-PEG^{1000} (Fig. 5d), the $u_{as}(PO^-_2)$ band was found in about the same position as in PE-PEG^{350} but there was an inversion of the peak orientation from negative to positive in the PM-IRRAS spectrum upon compression of the monolayer at π > 15 mN/m. The C=O band intensity also increased on compression. The signal corresponding to the PEG moiety was observed at 1126 cm^{-1} (ν_{as}(C—O-C)), with improved resolution at the highest pressure assayed.

3.6.1.3. PE-PE^{5000}. The peak of phosphate in the PM-IRRAS spectra of PE-PEG^{5000} monolayers was not clearly resolved at 5 mN/m, but appeared as a positive signal located at 1265 cm^{-1} when π reached 15 mN/m (Fig. 5e). Possibly because of its large molecular size, PEG induces a random orientation of the phospholipid moiety of the biopolymer. A peak inversion of $u_{as}(PO^-_2)$ was observed from positive at 15 mN/m to negative at 32 mN/m (Fig. 5e). At high π, the characteristic signal of PEG at 1100 cm^{-1} (ν_s(C—O—C)) could be distinguished, reflecting the acquisition of a less isotropic behavior

due to its higher degree of compaction. This is the main effect of molecular packing on the PM-IRRAS spectrum of PE-PEG^{5000} and distinguished this compound from the other two LPs studied.

3.6.2. Molecular orientation and organization of PE-PEGs at the water-air interface

PM-IRRAS can distinguish changes in the molecular surface density and orientation of transition dipoles. In our system, the $u_{as}(PO^{-}{}_2)$ peak increased from 1253 cm^{-1} in pure dpPE (Fig. 5a) to 1273 cm^{-1} in the case of PE-PEG^{350} (Fig. 5c), which clearly reflects a lower degree of hydration of the phosphate group in the lipopolymer. This is consistent with the fact that the $PO^{-}{}_2$ is not free in the lipopolymer as it is in dpPE, and may experience steric restrictions to becoming properly hydrated due to the presence of PEG chains.

The normalized quantity $I \times A$ for the $u_{as}(PO^{-}{}_2)$ peak from PE-PEG^{350}, PE-PEG^{1000} and PE-PEG^{5000} spectra was plotted vs. A (Fig. 1a–c). This procedure removed the contribution to I of the molecular density increase during compression, and revealed the true molecular reorientation. The decrease in I × A revealed that, on average, the $u_{as}(PO^{-}{}_2)$ transition vector, in all the PEG derivatives studied, turns with a more parallel orientation upon compression with respect to the monolayer normal. At ~32 mN/m, PE-PEG^{350} and PE-PEG^{5000} reached a similar $I \times A$ value (~ 65 Å^{-2}), and the slopes of the $I \times A$ change with respect to A, upon compression from 5 to 30 mN/m, were within the same order of magnitude (−0.170 and −0.125, respectively). The $PO^{-}{}_2$ transition dipole seems more vertically oriented in PE-PEG^{1000} compared to the other PEG derivatives ($I \times A \cong 46$ Å^{-2} at 35 mN/m) and, interestingly, a discontinuity appeared in this LP in $I \times A$ at a molecular area corresponding to "t2" (the slope of the $I \times A$ vs. A plot changed from −0.089 to +0.95 at "t2"). This behavior might be associated with bond rotation forced by the packing of polymeric tails.

4. Conclusions

In the present work, the use of a PEG-grafted phospholipid covering a wide range of polymer chain lengths highlighted the important role played by molecular geometry (derived from the molecular area at the closest packing) in defining molecular packing-dependent interfacial organization (Fig. 6a). Two types of 2D-transitions, named t1 and t2, were observed in π-A compression isotherms and correlated with critical polymer chain lengths (Fig. 6b), the former showing up the onset of a geometrical transition in the polymer head at low π and the latter limiting polymeric tail compaction at high π. This behavior resembles that of O-linked alkyl glycerol derivatives [13].

The thickness of PEG layers in several PE-PEG^n films has been shown to depend on the PE-PEG^n molecular density as well as on the polymeric chain length [2,47,48]. This is in accordance with present data from PM-IRRAS (e.g., increase in ν_s(C—O—C) band intensity upon compression, Fig. 5) and surface potential changes ($\Delta\Delta V$, Fig. 1). Moreover, it is known that PEG^{6000} induces a decrease in the dielectric constant (ε) of water [49,50], which can be explained by a high proportion of non-polarizable water in PEG^{6000} solutions [51] as well as in the dispersion of functionalized PEG-lipid vesicles [30]. In line with this, we show here that the PEG layer of LP monolayers provided a hydrophobic environment for DiIC18 in EFM and a low degree of hydration of the phosphate group in LPs, as revealed by PM-IRRAS. Taking together the direct correlation between PEG chain length, polymer layer thickness, packing density and hydrophobicity (low ε), an association can be made between the polymeric layer of a LP film and the dielectric in a capacitor (see Section 7, Supplementary material), making it possible to predict the behavior of the former as an electrical insulating layer.

The π value at which the orientation of the $PO_2{}^{-}$ transition dipole changes with respect to the interface anticipates the conformational transitions that occur in the HC ("t2"). A sol-gel transition within the hydrophilic layer is a feasible explanation that may be applied for both PE-PEG^{1000} and PE-PEG^{5000}. Several pieces of evidence support this hypothesis: EFM images, our previous results from NMR of water structure within PEG environments [30,51], rheological transitions observed in lipopolymeric matrices indicative of polymer gelation [19,52] and the significant increase in C—O—C signal intensity in PM-IRRAS spectra upon compression (Fig. 5d, e, present work). At "t2", the formation occurred of a two-dimensional physical network of LP through two different types of associative interactions: a) microcondensation of alkyl chains into small LP groups, and b) hydrogen-bonding through water molecules that link adjacent PEG molecules while the free water is displaced. This phenomenon leads to the emergence of 2D-aggregate-like structures at the mesoscopic level at/above "t1", which appeared only if the polymeric moiety reached a threshold size (MW ≫350 in the present series studied).

Two main concepts emerged from the results, i.e. a correlation between molecular geometry and interfacial behavior of LP, and the existence of two critical lengths of polymer chains, one of them allowing the onset of a transition at low π and the other limiting HC compaction at high π. In conjunction, these may be important for designing lipopolymeric self-aggregating structures, e.g. vesicles for drug delivery, simulating a biomembrane with glycocalix or building electrical biosensors. However, if they are to be used in biological media, the effect of ionic solutions on the packing density of LPs molecules reported previously [53], as well as an effect of ions on the water structure [54], should be taken into account.

Acknowledgments

The authors gratefully acknowledge the help of Dr R. Oliveira of CIQUIBIC (CONICET-Fac Cs Químicas, Universidad Nacional de Córdoba) with BAM experiments. The work was supported by grants from CONICET, SeCyT-UNC, and ANPCyT. NAC is a fellowship holder, and EMC and MAP are career members of CONICET (Argentina).

Appendix A. Supplementary data

Supplementary data associated with this article can be found, in the online version, at http://dx.doi.org/10.1016/j.colsurfb.2016.09.023.

References

[1] D.G. Zhu, M.C. Petty, Langmuir 8 (1992) 619–623.
[2] V. Tsoukanova, C. Salesse, J. Phys. Chem. B 108 (2004) 10754–10764.
[3] J.P. Coffman, C.A. Naumann, Macromolecules 35 (2002).
[4] E.P. Enriquez, S. Granick, Colloids Surf. A 113 (1996) 11–17.
[5] J.-Y. Kim, J.-K. Kim, J.-S. Park, Y. Byun, C.-K. Kim, Biomaterials 30 (2009) 5751–5756.
[6] M.C. Woodle, D.D. Lasic, Biochim. Biophys. Acta 1113 (1992) 171–199.
[7] M.F. Schneider, K. Lim, G.G. Fuller, M. Tanaka, Phys. Chem. Chem. Phys. 4 (2002) 1949–1952.
[8] T.R. Baekmark, G. Elender, D.D. Lasic, E. Sackmann, Langmuir 11 (1995) 3975–3987.
[9] M.C. Faure, P. Bassereau, L.T. Lee, A. Menelle, C. Lheveder, Macromolecules 32 (1999) 8538–8550.
[10] J. Lecourtier, R. Audebert, C. Quivoron, Macromolecules 12 (1979) 141–146.
[11] D. Marsh, R. Bartucci, L. Sportelli, Biochim. Biophys. Acta 1615 (2003) 33–59.
[12] G.G. Fuller, Rheology of mobile interfaces, in: Rheology Reviews, The British Society of Rheology, 2003, pp. 77–123.
[13] G. Mathe, C. Gege, K.R. Neumaier, R.R. Schmidt, E. Sackmann, Langmuir 16 (2000) 3835–3845.
[14] T.R. Baekmark, T. Wiesenthal, P. Kuhn, A. Albersdarfer, O. Nuyken, R. Merkel, Langmuir 15 (1999) 3616–3626.
[15] V. Tsoukanova, C. Salesse, Langmuir 24 (2008) 13019–13029.
[16] D.T. Auguste, J. Kirkwood, J. Kohn, G.G. Fuller, R.K. Prud'homme, Langmuir 24 (2008) 4056–4064.

[17] M. Winterhalter, H. Bürner, S. Marzinka, R. Benz, J.J. Kasianowicz, Biophys. J. 69 (1995) 1372–1381.
[18] T. Wiesenthal, T.R. Baekmark, R. Merke, Langmuir 15 (1999) 6837–6844.
[19] C.A. Naumann, C.F. Brooks, G.G. Fuller, T. Lehmann, J. Ruhe, W. Knoll, P. Kuhn, O. Nuyken, C.W. Frank, Langmuir 17 (2001) 2801–2806.
[20] A.K. Kenworthy, S.A. Simon, T.J. McIntosh, Biophys. J. 68 (1995) 1903–1920.
[21] M.G. Theumer, P.D. Clop, H.R. Rubinstein, M.A. Perillo, J. Phys. Chem. B 116 (2012) 14216–14227.
[22] D. Blaudez, J.M. Turlet, J. Dufourcq, D. Bard, T. Buffeteau, B. Desbat, J. Chem. Soc. Faraday Trans. 92 (1996) 525–530.
[23] L. Mao, A.M. Ritcey, B. Desbat, Langmuir 12 (1996) 4754–4759.
[24] M.A. Perillo, A. Polo, A. Guidotti, E. Costa, B. Maggio, Chem. Phys. Lipids 65 (1993) 225–238.
[25] J.T. Davies, E.K. Rideal, Interfacial Phenomena, Second ed., Academic Press Inc, New York, 1963.
[26] V. Tsoukanova, C. Salesse, Macromolecules 36 (2003) 7227–7235.
[27] N. Vila-Romeu, M. Nieto-Suárez, M. Broniatowski, Thin Solid Films 516 (2008) 8852–8859.
[28] T. Baumgart, G. Hunt, E.R. Farkas, W.W. Webb, G.W. Feigenson, BBA Biomembr 1768 (2007) 2182–2194.
[29] E.M. Clop, Modulación de la actividad de la fosfatasa alcalina placentaria inducida por la organización dinámica de su entorno molecular, Depto de Química, Universidad Nacional de Córdoba, Córdoba, 2010, pp. 111.
[30] E.M. Clop, A.K. Chattah, M.A. Perillo, J. Phys. Chem. B 118 (2014) 6150–6158.
[31] Y. Kim, J. Pyun, J.M.J. Frachet, C.J. Hawker, C.W. Frank, Langmuir 21 (2005) 10444–10458.
[32] H. Ahrens, T.R. Baekmark, R. Merkel, J. Schmitt, G. Karlheinz, R. Raiteri, C.A. Helm, ChemPhysChem 2 (2000) 101–106.
[33] M.B. Foreman, J.P. Coffman, M.J. Murcia, S. Cesana, R. Jordan, G.S. Smith, C.A. Naumann, Langmuir 19 (2003) 326–332.
[34] M.C. Fauré, P. Bassereau, B. Desbat, Eur. Phys. J. B 2 (2000) 145–151.
[35] M.W.A. Skoda, R.M.J. Jacobs, J. Willis, F. Schreiber, Langmuir 23 (2007) 970–974.
[36] W. Hubner, H.H. Mantsch, Biophys. J. 59 (1991) 1261–1272.
[37] T. Buffeteau, D. Blaudez, E. Pere, B. Desbat, J. Phys. Chem. B 103 (1999) 5020–5027.
[38] R.A. Dluhy, J. Phys. Chem. B 90 (1986) 1373–1379.
[39] J. Saccani, S. Castano, B. Desbat, D. Blaudezy, Biophys. J. 85 (2003) 3781–3787.
[40] D. Blaudez, T. Buffeteau, J.C. Cornut, B. Desbat, N. Escafre, M. Pezolet, J.M. Turlet, Appl. Spectrosc. 47 (1993) 869–874.
[41] S. Leekumjorn, A.K. Sum, Biophys. J. 90 (2006) 3951–3965.
[42] R.N.A.H. Lewis, R.N. McElhaney, Chem. Phys. Lipids 96 (1998) 9–21.
[43] S.H. Almaleck, F. Lairion, E.A. Disalvo, G.J. Gordillo, Chem. Phys. Lipids 139 (2006) 50–156.
[44] J. Castresana, J.L. Nieva, E. Rivas, A. Alonso, Biochem. J. 282 (1992) 467–470.
[45] P.T.T. Wong, H.H. Mantsch, Chem. Phys. Lipids 46 (1988) 213–224.
[46] G.D. Smith, D. Bedrov, O. Borodin, J. Am. Chem. Soc. 122 (2000) 9548–9549.
[47] T.L. Kuhl, J. Majewski, P.B. Howes, K. Kjaer, A. von Nahmen, K.Y.C. Lee, B. Ocko, J.N. Israelachvili, G.S. Smith, J. Am. Chem. Soc. 121 (1999) 7682–7688.
[48] H. Bianco-Peled, Y. Dori, J. Schneider, L.-P. Sung, S. Satija, M. Tirrell, Langmuir 17 (2001) 6931–6937.
[49] O. Zschörnig, S. Ohki, Gen. Physiol. Biophys. 12 (1993) 259–269.
[50] K. Arnold, A. Herrmann, L. Pratsch, K. Gawrisch, Biochim. Biophys. Acta 815 (1985) 515–518.
[51] E.M. Clop, M.A. Perillo, A.K. Chattah, J. Phys. Chem. B 116 (2012) 11953–11958.
[52] C.A. Naumann, C.F. Brooks, G.G. Fuller, W. Knoll, C.W. Frank, Langmuir 15 (1999).
[53] M.N. Shahid, V. Tsoukanova, J. Phys. Chem. B 115 (2011) 3303–3314.
[54] Q.A. Besford, M. Liu, A. Gray-Weale, Phys. Chem. Chem. Phys. 8 (2016) 14949–14959.